

Etched ion-track membranes as tailored separators in Li–S batteries

Pui Lap Jacob Lee^{1,2} , Vigneshwaran Thangavel^{3,4}, Claude Guery^{3,4},
Christina Trautmann^{1,2}, Maria Eugenia Toimil-Molares^{1,*} and
Mathieu Morcrette^{3,4,*}

¹ Materialforschung, GSI Helmholtzzentrum für Schwerionenforschung, Planckstraße 1, D-64291 Darmstadt, Germany

² Material- und Geowissenschaften, Technische Universität Darmstadt, Alarich-Weiss-Straße 2, D-64287 Darmstadt, Germany

³ Laboratoire de Réactivité et Chimie des Solides UMR CNRS 7314, 15 rue Baudelocque, F-80000 Amiens, France

⁴ Réseau sur le Stockage Electrochimique de l'Energie (RS2E), FR CNRS n°3459, France

E-mail: m.e.toimilmolares@gsi.de and mathieu.morcrette@u-picardie.fr

Received 1 March 2021, revised 6 May 2021

Accepted for publication 24 May 2021

Published 14 June 2021



CrossMark

Abstract

Lithium–sulfur (Li–S) batteries are considered a promising next generation alternative to lithium-ion batteries for energy storage systems due to its high energy density. However, several challenges, such as the polysulfide redox shuttle causing self-discharge of the battery, remain unresolved. In this paper, we explore the use of polymer etched ion-track membranes as separators in Li–S batteries to mitigate the redox shuttle effect. Compared to commercial separators, their unique advantages lie in their very narrow pore size distribution, and the possibility to tailor and optimize the density, geometry, and diameter of the nanopores in an independent manner. Various polyethylene terephthalate membranes with diameters between 22 and 198 nm and different porosities were successfully integrated into Li–S coin cells. The reported coulombic efficiency of up to 97% with minor reduction in capacity opens a pathway to potentially address the polysulfide redox shuttle in Li–S batteries using tailored membranes.

Keywords: lithium–sulfur battery, polysulfide redox shuttle, etched ion track membrane, polyethylene terephthalate, PET, battery separator

(Some figures may appear in colour only in the online journal)


1. Introduction

Lithium–sulfur (Li–S) batteries are considered a promising next generation alternative to the current generation of lithium-ion batteries. In terms of energy, Li–S systems offer a far higher theoretical gravimetric energy density (2567 Wh kg^{−1}) than state-of-the-art lithium-ion systems (387 Wh kg^{−1}), taking

into account the electroactive mass [1]. Sulfur is cheap and abundant, being a side-product of the crude oil refinement process. The double effect of potentially lowered cost and higher energy density make Li–S batteries incredibly attractive for future development.

Considerable research effort has been devoted to overcome the challenges facing Li–S batteries, including self-discharge [2–4], lithium dendrite formation on the lithium metal anode [5, 6], and the effect known as the polysulfide redox shuttle [7, 8]. The issues of the self-discharge and the polysulfide redox shuttle owe their origins to the soluble nature of the lithium polysulfides (S_x^{2−}, 2 ≤ x ≤ 8). At the cathode, long chain polysulfide molecules are formed as intermediate products, which diffuse to and react with the

* Authors to whom any correspondence should be addressed.

 Original content from this work may be used under the terms of the [Creative Commons Attribution 4.0 licence](https://creativecommons.org/licenses/by/4.0/). Any further distribution of this work must maintain attribution to the author(s) and the title of the work, journal citation and DOI.

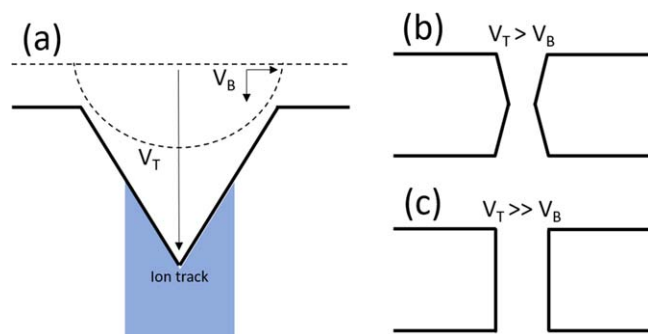


Figure 1. Scheme of track etching process where etching along the track V_T competes with isotropic bulk etching V_B (a). Resulting channel geometry depends on V_T/V_B ratio: bi-conical channels (b) and cylindrical channels (c).

lithium anode, forming lower order polysulfide molecules Li_2S_x , and diffusing back to the cathode again [9]. This shuttling of the molecules between the two sides is one of the causes of the lithium–sulfur system’s severe self-discharge, which lowers its coulombic efficiency. Some examples of strategies to mitigate this effect include modifying the cathode or using additives to trap the produced polysulfides and prevent their diffusion out of the cathode [10–12], modifying the separator in order to bind or prevent the movement of the polysulfides towards the anode [13–15], using metal-organic framework membranes as ionic sieves [16, 17], using intrinsically microporous polymer membranes to control polysulfide diffusion [18, 19], and using functionalized ion-selective polymers as membranes [20, 21].

Commercial separators in lithium-ion batteries are typically made of stretched polymer films such as polyethylene and polypropylene. They exhibit thicknesses on the order of tens of micrometers and large porosities with pore diameters on the order of micrometers. The large porosity is attained by stretching the polymer film, resulting in large distributions of the pore sizes and geometries.

Etched ion-track membranes, in turn, exhibit a very narrow pore size distribution, and density, geometry, and diameter of the nanopores can be tailored and adjusted in an independent manner. Etched ion-track membranes are formed by irradiating polymer foils with highly energetic heavy ions, followed by wet chemical etching. The technique is based on the fact that an individual heavy ion creates a cylindrical damaged zone along its trajectory, the so-called ion track. Within this ion track, the polymer’s chemical and physical properties are severely modified [22, 23]. By immersing the irradiated foil in an appropriate etchant, ion tracks are selectively dissolved and converted into open micro or nanochannels [24]. For the successful fabrication of membranes, the etching rate along the ion track, V_T , must be higher than the isotropic etching rate of the undamaged bulk material, V_B (figure 1(a)). The material of choice and the etching conditions (temperature, composition, and concentration of the etchant) determine the track-to-bulk etching ratio (V_T/V_B) and therefore also the geometry of the channels [25, 26]. Under symmetric etching conditions, low V_T/V_B ratios result in the formation of bi-conical channels

(figure 1(b)), while high V_T/V_B ratios result in the formation of cylindrical channels (figure 1(c)). High etching selectivity for ion tracks in polyethylene terephthalate (PET) is achieved by using sodium hydroxide (NaOH) solution [23]. Exposure of ion-irradiated polymers to UV light prior to etching increases V_T and leads to a narrower size distribution of the channels [27–29]. Under suitable fabrication conditions, membranes with monodispersed nanochannels can be fabricated [26]. Etched ion-track membranes can be obtained commercially and are widely used in filtration, surface protection, and biology. However, the application of etched ion-track membranes as separators in batteries has not been pursued until now [30].

In this work, we apply PET etched ion-track membranes with monodispersed cylindrical channels as separators in Li–S batteries. We compare the overall performance of Li–S batteries as a function of the channel size and pore density of the PET membranes. PET membranes are also applied to study the diffusion of polysulfides as a function of nanochannel size. We postulate that by applying polymer membranes with optimized porosity and channel size, the shuttle of polysulfide molecules between cathode and anode can be restricted while maintaining a sufficient transport of lithium ions. The results show that Li–S batteries assembled with an additional PET ion-track membrane exhibit improved coulombic efficiency compared to reference batteries assembled only with a commercial separator.

2. Methods

2.1. Synthesis of etched ion-track membranes

Commercial PET foils (Hostaphan RN, 19 μm thick, 3 cm diameter) were irradiated with 2 GeV gold ions at the universal Linear Accelerator (UNILAC) of the GSI Helmholtz Center for Heavy Ion Research. The foils were irradiated under perpendicular incidence, and the irradiation fluence was varied between 10^7 and 10^9 ions cm^{-2} with an accuracy of about $\pm 20\%$. Each ion creates along its trajectory in the PET foil, a cylindrical damage zone called an ion track [22, 23]. Before chemical etching, each side of the irradiated foils was exposed to ultraviolet light (Vilber Lourmat UV tube, 312 nm peak wavelength) for three hours. This process sensitizes the ion tracks created by the ions, yielding membranes with a narrow pore size distribution [27–29]. Track etching was performed by immersing the irradiated and sensitized PET foils in an aqueous solution of 6 M NaOH at 50 $^\circ\text{C}$. Under these conditions, the anisotropic etching rate of the material along the damaged ion-track is much higher than the isotropic etching rate of the bulk undamaged material, resulting in high aspect ratio cylindrical channels (figure 1). The resulting channel diameter was adjusted between 22 and 198 nm by selecting etching times between 60 and 330 s. The thickness of the PET membrane during etching decreases only by the corresponding pore diameter. After etching, the PET membranes were rinsed in distilled deionized water. Prior to their assembly in Li–S batteries, the etched membranes were

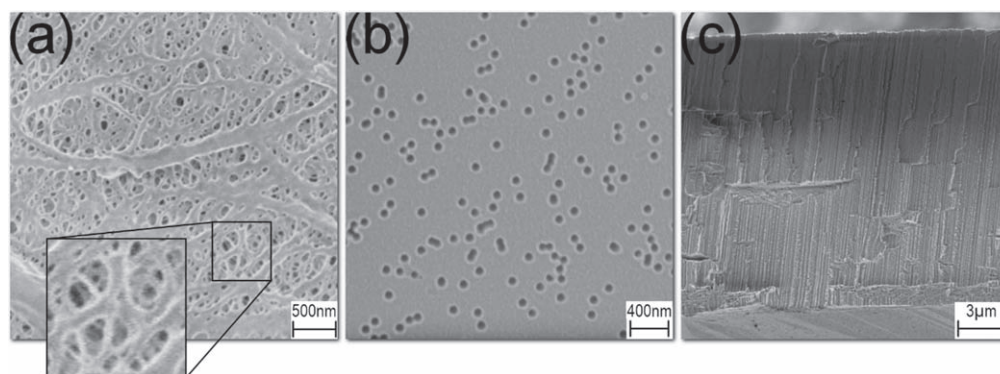


Figure 2. Representative SEM image of (a) a SK Innovation separator, (b) surface view of PET etched ion-track membrane with average pore diameter ~ 100 nm and pore density of $2.5 \times 10^9 \text{ cm}^{-2}$ (~ 25 pores per μm^2), and (c) cross section of PET membrane displaying parallel oriented nanochannels (average pore diameter ~ 93 nm, pore density 10^9 cm^{-2}).

punched into discs with a diameter of 1.6 cm and dried at 70°C under vacuum for 24 h.

Typical commercial battery separators exhibit poly-dispersed pores of irregular shapes and sizes on the order of up to micrometers [31]. Figure 2(a) shows an exemplary scanning electron microscopy (SEM) image of a SK innovation separator. The ion-track membranes, on the other hand, exhibit parallel oriented, randomly distributed, high aspect ratio pores with cylindrical geometry and a narrow size distribution (figures 2(b)–(c)).

2.2. Synthesis of carbon–sulfur composite for cathode

To synthesize the sulfur cathode, mesoporous carbon and sulfur powder were first heat-treated for 24 h under 300°C and 60°C respectively to remove moisture. The two treated materials were then mixed in a 50:50 weight percentage mixture, ground in a mortar, and heated at 155°C for 6 h in a sealed autoclave to impregnate the mesoporous carbon with the sulfur. Mixing and sealing in the autoclave was performed under an argon atmosphere.

By mixing the carbon–sulfur composite with carbon Super-P, poly (vinylidene fluoride-hexafluoropropylene) (PVdF-HFP) and N-Methyl-2-pyrrolidone (NMP) a soft slurry was composed. Carbon Super-P is used to increase the electrical conductivity of the composite, while PVDF-HFP is a binder for the slurry that improves its mechanical properties. The slurry was then casted over a roughened aluminum foil at an elevated temperature of 40°C to prevent water adsorption from the atmosphere. The dried slurry casted foil is then cut into 8 mm diameter circular discs to be later integrated as cathodes into the coin cells. Each disc contains 37.5% of sulfur by weight and is weighted to find the sulfur mass per cathode before cell assembly.

2.3. Cell assembly and testing

The PET membranes were integrated into Li–S coin cells to test their cycling performance. The PET membrane is sandwiched between two SK Innovation separators, which acted as a reservoir for the electrolyte. The electrolyte used was 1 M lithium bis(trifluoromethanesulfonyl)imide (LiTFSI) in

TEGDME:1,3-Dioxolane 1:1 by volume percentage solution. Electrolyte volume to sulfur mass ratio is a relative property, the dissolution of polysulfides and the polysulfide shuttle effect increase with this ratio regardless of the mass percentage of sulfur in the electrode. As this work focuses on the tailoring of the PET membrane to limit the shuttle effect, a high electrolyte volume to sulfur mass of ratio of $20 \mu\text{l mg}^{-1}$ was utilized in the cells. Each cathode was weighted before cell assembly to calculate the sulfur content, and thus the needed electrolyte volume. Coin cells were assembled with each layer in quick succession, starting with a carbon–sulfur cathode, the separator with reservoirs (SK separator/track-etched PET membrane/SK separator with half the electrolyte volume pipetted on each SK separator), and a lithium foil anode (figure 3). The cell was assembled in an argon glovebox and sealed in a coin cell before cycling. Cycling commenced as soon as possible after sealing the cell (< 10 min). Cycling of the coin cells was performed at a C-rate of C/10, under galvanostatic cycling with potential limitation from 1.5 to 3 V and at a constant temperature of 20°C . The polysulfide shuttle effect in Li–S batteries is mainly observed as overcharging during each cycle, whereas the capacity fading during cycling could be caused due to multiple phenomena such as detachment of lithium metal from the anode, electrolyte decomposition, or blockage of cathode pores. Therefore, we believe that the capacity fading during cycling is not the proper descriptor to prove the effectiveness of the ion-track membrane to restrict the shuttle effect and have limited the number of cycles to only 15. The decrease or the absence of overcharging of the cells which contain the etched ion-track membrane prove that they are effective in restricting the shuttle effect.

3. Results

To study the performance of the Li–S batteries as a function of the adjustable separator parameters, PET membranes with cylindrical channels with average diameters ranging from 22 to 198 nm (± 10 nm) and channel densities between 1×10^7 and $1 \times 10^9 \text{ cm}^{-2}$ were integrated into coin cells. The pore

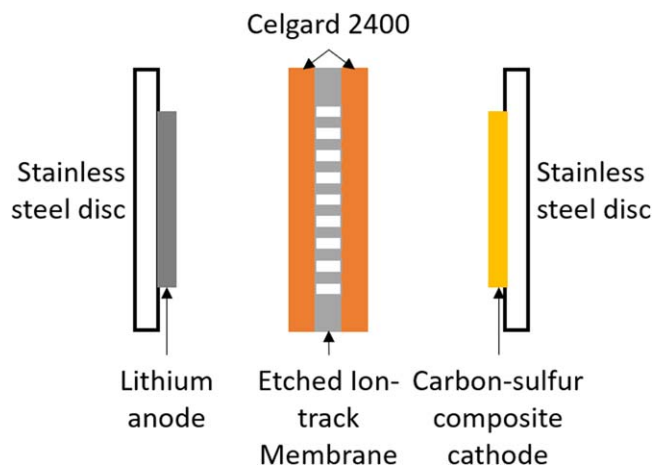


Figure 3. Exploded view of the different components in the coin cell. The separator configuration between the Li anode and the carbon-sulfur cathode consists of the track-etched PET membrane sandwiched between two SK Innovation membranes soaked with electrolyte.

Table 1. Pore density, pore diameter and calculated effective porosity P_{eff} of etched ion-track membranes. The pore size is deduced from SEM images (uncertainty ± 10 nm).

Pore density F (cm^{-2})	Pore diameter (nm)	P_{eff} (%)
10^7	115	0.1
10^8	115	1.0
10^9	115	9.9
10^7	168	0.2
10^8	168	2.2
10^9	168	19.9
10^9	198	26.5
10^9	22	0.4

size and porosity of the different membranes are listed in table 1. The effective porosity (P_{eff}) is calculated according to the following formula which takes the possible overlapping of pores into account [32]:

$$P_{\text{eff}} = 1 - e^{-FA},$$

where FA denotes the nominal porosity. F is the pore density which corresponds to the fluence applied during ion irradiation (number of impinging ions per cm^2), because each individual ion produces a track. A is the pore cross section ($A = \pi \cdot r^2$, with r being the channel radius). The pore density is measured by SEM, by counting the number of pores in a given area. The homogeneity of the pore density is typically within 10%–20%.

As reference, control cells were assembled with only one SK Innovation separator and without the track-etched PET membrane. For clarity, only one curve by each type of membrane is presented here. Tests of etched ion-track membranes with 10^9 channels cm^{-2} and average channel diameter of 22 nm showed no discharge, even after 24 h, and thus were not further investigated.

Figure 4 shows the specific charge and discharge capacity (a) and the coulombic efficiency (b) recorded for Li–S

cell coins assembled with PET membranes with 10^9 channels cm^{-2} and average channel diameters 115 nm (red), 168 nm (blue), and 198 nm (green) together with the reference cell (black).

The data shows that the coin cell assembled with the PET membrane with channels of ~ 115 nm exhibits a starting discharge capacity of 822 mAh g^{-1} and drops to 726 mAh g^{-1} by the 15th cycle. By comparison, the reference coin cell exhibits a starting discharge capacity of 1311 mAh g^{-1} , dropping to 850 mAh g^{-1} by the 15th cycle. There is also a significant 14% improvement of the coulombic efficiency from $\sim 83\%$ of the reference cell to 97% for the coin cell containing the PET membrane with channels of ~ 115 nm. We attribute this increase to a reduction of the polysulfide redox shuttle by the presence of the PET membrane with small monodispersed cylindrical channels. As the data shows, this increase comes at the cost of a reduced discharge capacity, caused by the decrease in porosity. An increase in the average channel diameter of the PET membrane from 115 to 168 nm and 191 nm (corresponding to a porosity of 19.9% and 24.9%, respectively) resulted in higher specific charge and discharge capacities. This is expected because the higher porosity yields a higher lithium conductivity, as well as lower coulombic efficiencies. The positive effect of the membrane with 115 nm pores on the coulombic efficiency can have several origins that are currently being discussed and investigated. Interaction between the polysulfides and the pore walls possibly affects the passage of the polysulfides from the cathode to the anode. PET nanopores are ion-selective under certain conditions [33].

The PET membrane is thus able to compare favorably efficiency-wise ($\sim 97\%$) to other polysulfide-blocking polymeric membranes reported in literature. As points of comparison, an ion-selective lithiated Nafion ionomer membrane reported by Jin *et al* exhibited coulombic efficiencies per cycle of above 97% [20], and a polymer with intrinsic nanoporosity membrane reported by Yu *et al* exhibited coulombic efficiencies of 99.72% [19].

Figure 5 shows the cycling performance of coin cells assembled with PET membranes with average channel diameter 115 nm and various channel densities, namely 10^7 cm^{-2} (red squares), 10^8 cm^{-2} (blue circles), and 10^9 cm^{-2} (green diamonds). In this case, after 15 cycles, the coulombic efficiencies of the three cells are very similar (95%–99%). However, the cells assembled with PET membranes with channel densities of 10^8 cm^{-2} and 10^7 cm^{-2} exhibit much lower charging and discharging capacities. The lower capacity for the membrane with 10^7 pores cm^{-2} suggests that the lower pore densities limit the transport of lithium ions between the anode and cathode.

Figure 6 displays the cycling performance of coin cells assembled with PET membranes with a larger average channel diameter of 168 nm and the same three different channel densities, 10^9 cm^{-2} (green diamonds), 10^8 cm^{-2} (blue circles), and 10^7 cm^{-2} (red squares). In figure 6(a), the cells with membranes with 10^9 channels cm^{-2} and porosity of 19.9% exhibit charging and discharging capacities of similar value to those of the reference cell (figure 4(a)). Reducing the

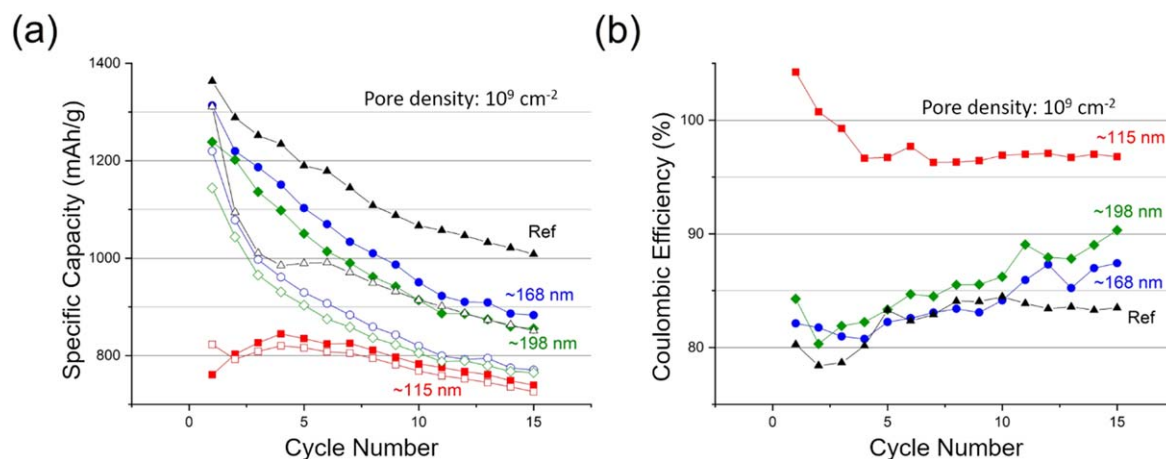


Figure 4. Cycling performance of Li-S coin cells with PET etched ion-track membrane sandwiched between two SK innovation separators for fixed pore density (10^9 cm^{-2}) and varying pore diameter. (a) Charge (solid symbols) and discharge (empty symbols) capacities, and (b) coulombic efficiencies of average pore diameter: 115 nm (red squares), 168 nm (blue circles), 198 nm (green diamonds), reference coin cell without track-etched membrane (black triangles).

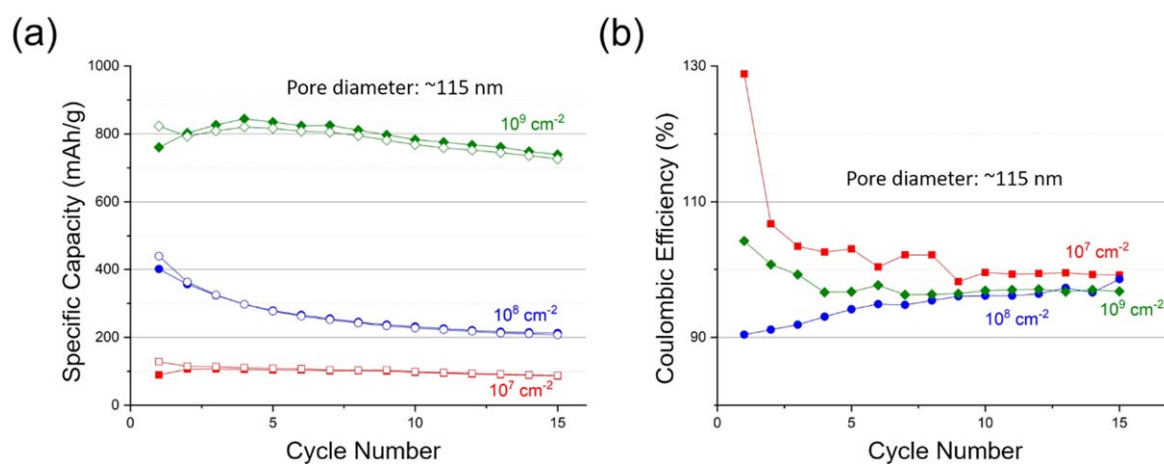


Figure 5. Cycling performance of Li-S coin cells with PET etched ion-track membrane sandwiched between two SK innovation separators for fixed pore diameter of ~115 nm and various pore densities. (a) Charge (solid symbols) and discharge (empty symbols) capacities, and (b) coulombic efficiencies of pore densities: 10^7 cm^{-2} (red squares), 10^8 cm^{-2} (blue circles), and 10^9 cm^{-2} (green diamonds).

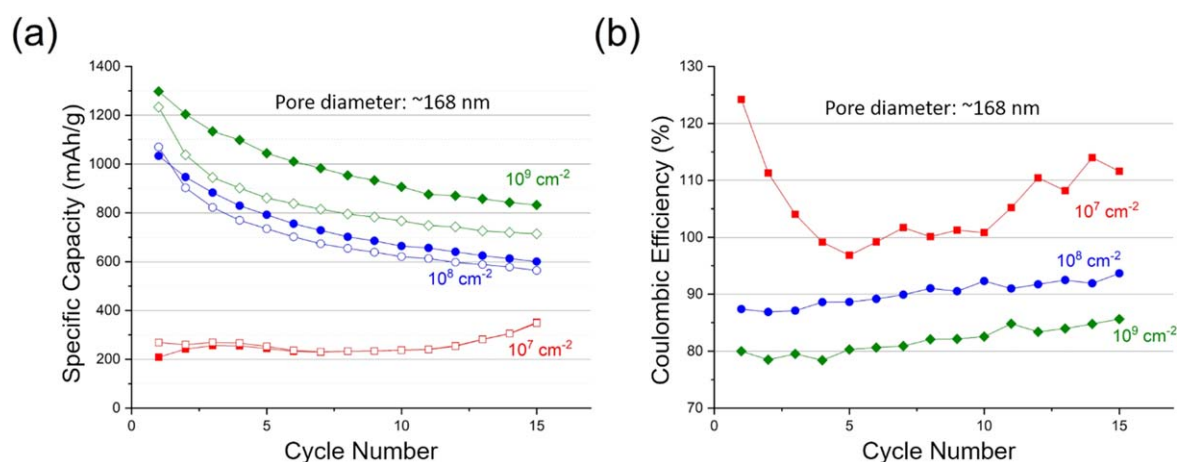


Figure 6. Cycling performance of Li-S coin cells with PET etched ion-track membrane sandwiched between two SK innovation separators for fixed pore diameter of ~168 nm and varying pore density. (a) Charge (solid symbols) and discharge (empty symbols) capacities, and (b) coulombic efficiencies of pore densities: 10^7 cm^{-2} (red squares), 10^8 cm^{-2} (blue circles), and 10^9 cm^{-2} (green diamonds).

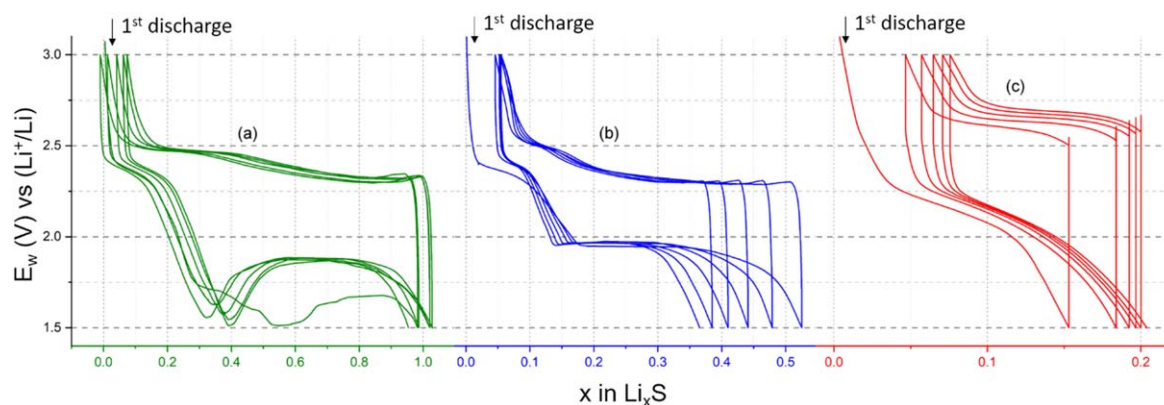


Figure 7. Cycling curves of the first 5 cycles for Li-S coin cells with 115 nm diameter channels and (a) 10^9 cm^{-2} (green), (b) 10^8 cm^{-2} (blue), and (c) 10^7 cm^{-2} pore densities. The arrows indicate the start of the cycling procedure. The x -axis is scaled differently for each curve.

channel density tenfold to 10^8 cm^{-2} reduced the charge and discharge capacities by about 150 mAh g^{-1} but increased the coulombic efficiency by 8%. Reducing the channel density further to 10^7 cm^{-2} cuts the capacity further to about 350 mAh g^{-1} at the 15th cycle.

Figure 7 shows the corresponding cycling curves of the first 5 cycles of these same coin cells. The cell with PET membrane of 10^9 cm^{-2} (figure 7(a)) shows only a small shift per cycle, corresponding to the relatively high coulombic efficiency of the cell. The cell with the PET membrane with 10^8 cm^{-2} channel density (figure 7(b)) shows a discharge curve with higher discharge potential, and a short discharge plateau, indicative of more restricted ionic flow. The discharge curve in figure 7(b) is also shorter than that of the charge curve in each cycle after the initial one, possibly due to the difficulty of lithium ions reaching the cathode due to the low porosity of the membrane. Further reducing the channel density to 10^7 cm^{-2} (figure 7(c)) shows much higher resistance between the cathode and anode. The discharge and charge plateaus are short, indicating that polysulfide concentration is low due to severely limited ionic flow, leading to sharply reduced capacity (figure 5(a)).

For all membranes with pore densities of 10^7 cm^{-2} , we measured coulombic efficiencies of the cells above 100%. This effect which appears with the initial cycles is likely due to the activation of sulfur, whereby more lithium ions in successive cycles are reaching sulfur that had not been utilized in any reaction during the previous cycles. This could be an indication that the low number of pores is severely reducing the ionic flow between the cathode and the anode such that the Li ions on the cathode side of the membrane are consumed faster than they can diffuse through the membrane from the anode. During each cycle, new Li ions would reach the carbon-sulfur cathode after diffusing through the membrane, driving up the coulombic efficiency.

These systematic studies of Li-S batteries assembled with an additional PET separator clearly indicate that the performance of the battery, i.e. capacity retention and coulombic efficiency, can be influenced by the porosity and channel diameter of separators with tailored channel

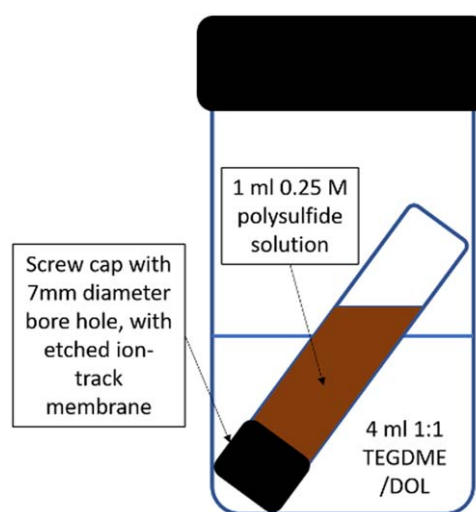


Figure 8. Etched ion-track membrane diffusion test setup. A screw cap with a 7 mm diameter bore hole in the middle and an etched ion-track membrane separates the polysulfide solution in the small vial from the pure solvent solution of 1:1 TEGDME: DOL.

parameters. The best performance was achieved for the PET separator with $d \sim 115 \text{ nm}$, and pore density 10^9 cm^{-2} .

To estimate the influence of the nanochannel diameter on the diffusion of the polysulfides in the batteries, $19 \mu\text{m}$ thick PET membranes, with a pore density of 10^9 cm^{-2} and with different average pore sizes were used to tightly close vials containing a 0.25 M nominal Li_2S_6 polysulfide solution. This corresponds to the concentration value expected in the coin cells tests if about all of the sulfur in the cell is converted to Li_2S_6 within the electrolyte (according to the employed $20 \mu\text{l}$ per mg of S). The vials were then inserted upside down in a pure solvent solution of 1:1 TEGDME: DOL, with the etched ion-track membranes being the only barrier between the polysulfide and the solvent solutions (figure 8).

The diffusion of polysulfide molecules along the nanochannels of the membrane caused by the concentration gradient was then monitored visually for 30 days, with photos taken hourly for the first 8 hours, and every 24 hours subsequently. Figure 9 shows the photographs taken for vials with PET membrane-separators with pore diameter $\sim 74 \text{ nm}$

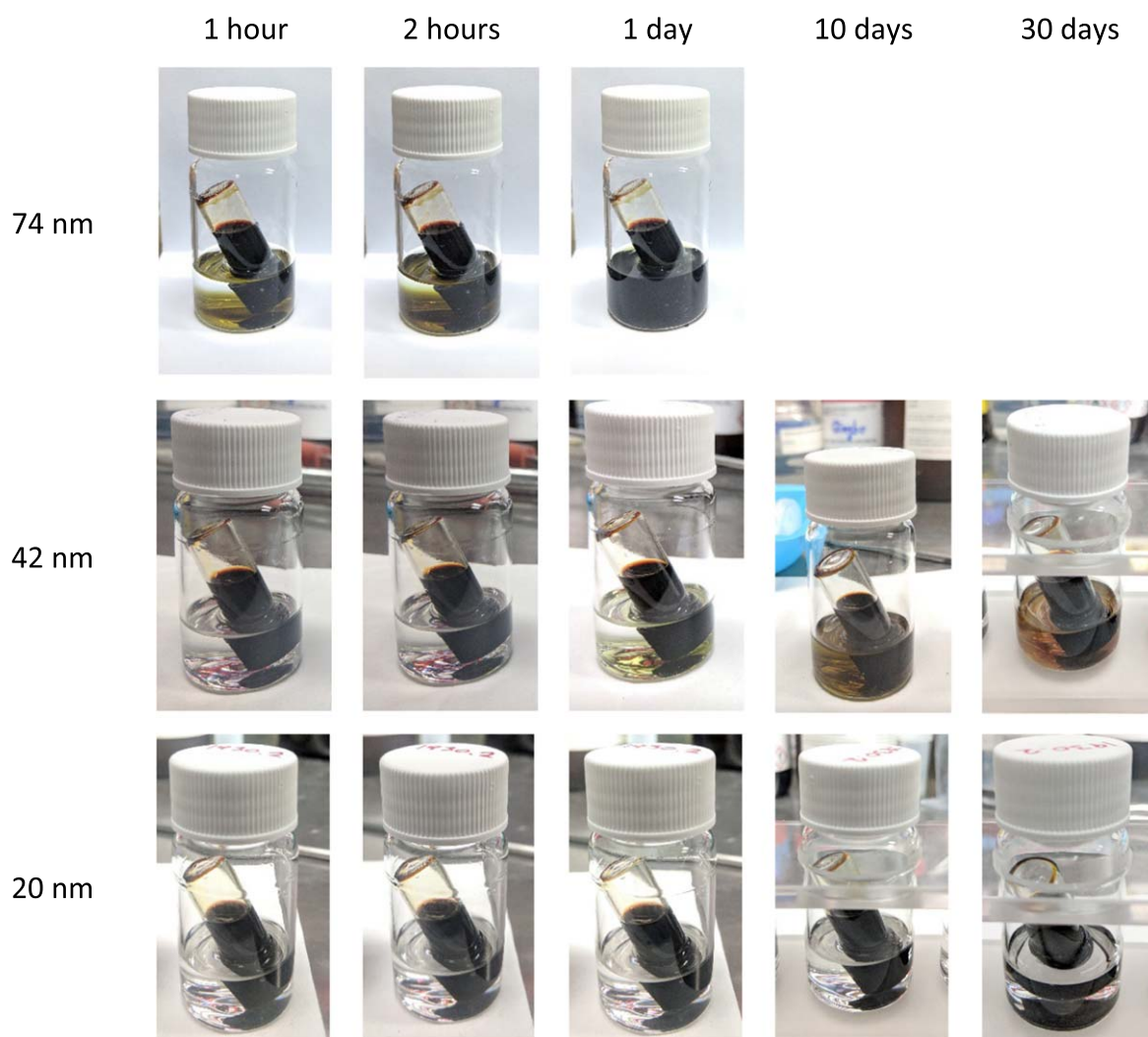


Figure 9. Polysulfide diffusion tests of membranes with fluence of 10^9 cm^{-2} and pore diameters 74 nm (top row), 42 nm (middle row), and 20 nm (lower row).

(top row), 42 nm (middle row) and 20 nm (lower row). The porosity of these three membranes varies between 4.2% and 0.3%. For all vials, there was no visually apparent change in the liquid levels for the polysulfide or the pure solvent solution during the course of the experiment. For the PET separators with largest nanochannels (diameter ~ 74 nm) the diffusion of the polysulfides across the membrane under this maximal concentration gradient happens relatively quickly, within 24 hours. For the PET separators with average pore diameter ~ 42 nm only a small amount of polysulfides diffused through during the first 24 hours, and even after 30 days, a certain concentration gradient is still present. Finally, reducing the average pore diameter down to 20 nm prevented the diffusion of the polysulfides through up to 30 days.

These diffusion experiments were performed under large polysulfide concentration gradients and indicate that the diffusion of lithium polysulfides can be strongly affected by proper tailoring of the separator nanochannel diameter. The better performance exhibited by some of the Li-S cells with PET separators compared to the reference one can be explained by a reduction of the lithium polysulfide diffusion,

due to a lack of an initial polysulfide concentration gradient in the coin cells. *In-situ* analysis of the Li-S cell during operation by Patel *et al* showed that evolution of polysulfides begins during the initial discharge, and their concentration increases and decreases with the charge and discharge cycles of the cell [34]. The results indicate that the presence of an ion-track membrane with monodispersed channels and optimized porosity in a Li-S battery can hinder the diffusion of the polysulfides across to the anode and improve the battery performance. Future experiments will be devoted to further optimization of channel diameter and porosity, as well as to the application of tailored membranes of other polymer materials.

4. Conclusion

The advantages of applying membranes with monodispersed channels and tailored parameters as separators in battery systems have been discussed. A systematic variation of the individual separator parameters in an independent manner

enables the investigation of diffusion and electrochemical processes involved, and thus the optimization of the separator parameters and the battery performance. Etched ion-track membranes with average pore diameters 115, 168, and 198 nm, and pore densities 10^7 , 10^8 , and 10^9 cm⁻² were tested. An increased coulombic efficiency was observed particularly for PET separators with porosities $\sim 10\%$ and pore diameter ~ 115 nm, pointing to a reduction of the problematic redox shuttle effect in lithium-sulfur batteries. Coulombic efficiency of up to 97% has been shown, with minor reduction in capacity compared to reference cells using commercial separators, namely ~ 800 mAh g⁻¹. Lithium polysulfide diffusion is significantly hindered for etched ion-track membranes with smaller channels and indicates that the application of such membranes could undermine the polysulfide shuttle redox effect, improving lithium-sulfur battery performance. Separators with optimized porosities, i.e. smaller pore diameters and higher pore densities are expected to further improve the Li-S battery performance.

Acknowledgments

P L J Lee would like to thank HGS-HiRe (Helmholtz Graduate School for Hadron and Ion Research) and the Stiftung Giersch for their financial support. Ion irradiations were performed at the X0-beamline of the UNILAC at the GSI Helmholtzzentrum für Schwerionenforschung, Darmstadt (Germany) in the frame of FAIR Phase-0.

Data availability statement

The data that support the findings of this study are available upon reasonable request from the authors.

ORCID iDs

Pui Lap Jacob Lee  <https://orcid.org/0000-0003-1664-4102>

References

- [1] Bruce P G, Scrosati B and Tarascon J-M 2008 Nanomaterials for rechargeable lithium batteries *Angew. Chem. Int. Ed.* **47** 2930–46
- [2] Sun M, Wang X, Wang J, Yang H, Wang L and Liu T 2018 Assessment on the self-discharge behavior of lithium-sulfur batteries with LiNO₃-possessing electrolytes *ACS Appl. Mater. Interfaces* **10** 35175–83
- [3] Knap V, Stroe D, Swierczynski M, Teodorescu R and Schaltz E 2016 Investigation of the self-discharge behavior of lithium-sulfur batteries *J. Electrochem. Soc.* **163** A911–6
- [4] Moy D, Manivannan A and Narayanan S R 2014 Direct measurement of polysulfide shuttle current: a window into understanding the performance of lithium-sulfur cells *J. Electrochem. Soc.* **162** A1–7
- [5] Cheng X-B, Huang J-Q and Zhang Q 2018 Review—Li metal anode in working lithium-sulfur batteries *J. Electrochem. Soc.* **165** A6058–72
- [6] Zhao H, Deng N, Yan J, Kang W, Ju J, Ruan Y, Wang X, Zhuang X, Li Q and Cheng B 2018 A review on anode for lithium-sulfur batteries: progress and prospects *Chem. Eng. J.* **347** 343–65
- [7] Busche M R, Adelhelm P, Sommer H, Schneider H, Leitner K and Janek J 2014 Systematical electrochemical study on the parasitic shuttle-effect in lithium-sulfur-cells at different temperatures and different rates *J. Power Sources* **259** 289–99
- [8] Zhang S S 2013 Liquid electrolyte lithium/sulfur battery: fundamental chemistry, problems, and solutions *J. Power Sources* **231** 153–62
- [9] Ji X and Nazar L F 2010 Advances in Li-S batteries *J. Mater. Chem.* **20** 9821
- [10] Li L et al 2017 Phosphorene as a polysulfide immobilizer and catalyst in high-performance lithium-sulfur batteries *Adv. Mater.* **29** 1–8
- [11] Sun Z, Zhang J, Yin L, Hu G, Fang R, Cheng H M and Li F 2017 Conductive porous vanadium nitride/graphene composite as chemical anchor of polysulfides for lithium-sulfur batteries *Nat. Commun.* **8** 1–8
- [12] Jia L, Wu T, Lu J, Ma L, Zhu W and Qiu X 2016 Polysulfides capture-copper additive for long cycle life lithium sulfur batteries *ACS Appl. Mater. Interfaces* **8** 30248–55
- [13] Shao H, Wang W, Zhang H, Wang A, Chen X and Huang Y 2018 Nano-TiO₂ decorated carbon coating on the separator to physically and chemically suppress the shuttle effect for lithium-sulfur battery *J. Power Sources* **378** 537–45
- [14] Ghazi Z A, He X, Khattak A M, Khan N A, Liang B, Iqbal A, Wang J, Sin H, Li L and Tang Z 2017 MoS₂/Celgard separator as efficient polysulfide barrier for long-life lithium-sulfur batteries *Adv. Mater.* **29** 1606817
- [15] Bugga R, Jones J P, Jones S C, Krause F C, Pasalic J, Ganapathi D S, Hendrickson M and Plichta E J 2018 New separators in lithium/sulfur cells with high-capacity cathodes *J. Electrochem. Soc.* **165** A6021–8
- [16] Bai S, Liu X, Zhu K, Wu S and Zhou H 2016 Metal-organic framework-based separator for lithium-sulfur batteries *Nat. Energy* **1** 16094
- [17] Zang Y, Pei F, Huang J, Fu Z, Xu G and Fang X 2018 Large-area preparation of crack-free crystalline microporous conductive membrane to upgrade high energy lithium-sulfur batteries *Adv. Energy Mater.* **8** 1802052
- [18] Li C, Ward A L, Doris S E, Pascal T A, Prendergast D and Helms B A 2015 Polysulfide-blocking microporous polymer membrane tailored for hybrid Li-sulfur flow batteries *Nano Lett.* **15** 5724–9
- [19] Yu X, Feng S, Boyer M J, Lee M, Ferrier R C, Lynd N A, Hwang G S, Wang G, Swinnea S and Manthiram A 2018 Controlling the polysulfide diffusion in lithium-sulfur batteries with a polymer membrane with intrinsic nanoporosity *Mater. Today Energy* **7** 98–104
- [20] Jin Z, Xie K, Hong X, Hu Z and Liu X 2012 Application of lithiated Nafion ionomer film as functional separator for lithium sulfur cells *J. Power Sources* **218** 163–7
- [21] Bauer I, Thieme S, Brückner J, Althues H and Kaskel S 2014 Reduced polysulfide shuttle in lithium-sulfur batteries using Nafion-based separators *J. Power Sources* **251** 417–22
- [22] Apel P Y 1995 Heavy particle tracks in polymers and polymeric track membranes *Radiat. Meas.* **25** 667–74
- [23] Apel P, Schulz A, Spohr R, Trautmann C and Vutsadakis V 1998 Track size and track structure in polymer irradiated by heavy ions *Nucl. Instrum. Methods Phys. Res. B* **146** 468–74
- [24] Fleisher R L, Price P B and Walker R M 1975 *Nuclear Tracks in Solids (Principles & Applications)* (Berkeley, CA: University of California Press)

- [25] Trautmann C, Bröchle W, Spohr R, Vetter J and Angert N 1996 Pore geometry of etched ion tracks in polyimide *Nucl. Instrum. Methods Phys. Res. B* **111** 70–4
- [26] Trautmann C, Bouffard S and Spohr R 1996 Etching threshold for ion tracks in polyimide *Nucl. Instrum. Methods Phys. Res. B* **116** 429–33
- [27] Zhu Z, Maekawa Y, Liu Q and Yoshida M 2005 Influence of UV light illumination on latent track structure in PET *Nucl. Instrum. Methods Phys. Res. B* **236** 61–7
- [28] Zhu Z, Maekawa Y, Koshikawa H, Suzuki Y, Yonezawa N and Yoshida M 2004 Role of UV light illumination and DMF soaking in production of PET ion track membranes *Nucl. Instrum. Methods Phys. Res. B* **217** 449–56
- [29] Cornelius T W, Schiedt B, Severin D, Pépy G, Toulemonde M, Apel P Y, Boesecke P and Trautmann C 2010 Nanopores in track-etched polymer membranes characterized by small-angle x-ray scattering *Nanotechnology* **21** 155702
- [30] Toimil-Molares M E, Trautmann C, Lee P L J and Morcrette M 2018 Porous etched ion-track polymer membrane as a separator for a battery (European Patent Office - EP3416211A1) (<https://data.epo.org/gpi/EP3416211A1>)
- [31] Zhang S S 2007 A review on the separators of liquid electrolyte Li-ion batteries *J. Power Sources* **164** 351–64
- [32] Spohr R 2009 Ion tracks for micro- and nanofabrication: from single channels to superhydrophobic surfaces *Digit. Compr. Summ. Uppsala Diss. Fac. Sci. Technol.* **700** 1–63
- [33] Apel P Y, Korchev Y E, Siwy Z, Spohr R and Yoshida M 2001 Diode-like single-ion track membrane prepared by electro-stopping *Nucl. Instrum. Methods Phys. Res. B* **184** 337–46
- [34] Patel M U M, Demir-Cakan R, Morcrette M, Tarascon J-M, Gaberscek M and Dominko R 2013 Li-S battery analyzed by UV/Vis in operando mode *ChemSusChem* **6** 1177–81